The Influence of Electronic Acupuncture At A Specific Frequency In Facilitating The Passage of NGF Through The Blood-Brain Barrier And Its Effect On Learning And Memory In MCAO/R Rats

Yibin Zhao
Zhejiang Chinese Medical University
Xuqing Mao
Zhejiang Chinese Medical University
Hao Wang
Zhejiang Chinese Medical University
Lin Gan
Zhejiang Chinese Medical University
Shanshan Zhang
Zhejiang Chinese Medical University
Peng Gong
Zhejiang Chinese Medical University
Xianming Lin (linxianming1966@163.com)
Zhejiang Chinese Medical University https://orcid.org/0000-0001-5031-7725

Research

Keywords: Electronic acupuncture, blood-brain barrier, MCAO, NGF

Posted Date: October 28th, 2021

DOI: https://doi.org/10.21203/rs.3.rs-1014162/v1

Version of Record: A version of this preprint was published at Journal of Integrative Neuroscience on April 8th, 2022. See the published version at https://doi.org/10.31083/j.jin2103079.

Abstract

The blood-brain barrier (BBB) maintains the balance of the internal environment of the brain and strictly controls substance exchange between the brain and blood dynamically but stably. Transient increases in the permeability of the BBB plays an important role in helping macromolecular drugs enter the brain to exert their pharmacological effects. Previous research has revealed that electronic acupuncture (EA) stimulation at a specific frequency can enhance the permeability of the BBB and induce the entry of 20 kDa fluorescein isothiocyanate-dextran (FITC-dextran) into the cerebral cortex, but whether it can also allow drugs to pass the BBB remains unknown. We hypothesized that EA at a specific frequency could open the BBB and induce the entry of nerve growth factor (NGF) into the brain to exert its therapeutic effect. To simulate the clinical apoplexy sequelae observed in patients and determine the basic timing of BBB repair under pathological conditions, we employed the middle cerebral artery occlusion (MCAO) model and assessed changes in the permeability and structure of the BBB by measuring both the intensity of Evans blue (EB) staining and the cerebral infarction volume and evaluating the ultrastructure of the BBB. Then, we used a laser spectrometer and immunofluorescence to observe entry of NGF into the brain. Finally, we assessed the learning and memory ability of rats and used the DeadEnd TM Fluorometric TUNEL System to assess apoptosis in the hippocampus. Our results showed that the BBB was essentially repaired three weeks after MCAO, indicating that EA stimulation at a specific frequency can enhance BBB permeability and induce NGF uptake by prefrontal neurons. In the presence of EA stimulation, entry of NGF into the brain promoted learning and memory in rats and inhibited the apoptosis of neurons in the hippocampus. In this study, the MCAO model was used to determine the timing of BBB repair under pathological conditions and assess the EA stimulation-induced entry of NGF into the brain to exert its therapeutic effect. EA could serve as a new strategy for delivering therapeutics to the central nervous system (CNS), given that EA stimulation at a specific frequency was shown to increase the permeability of the BBB. Further study of the mechanism underlying the opening of the BBB and its timing is needed.

Introduction

Ischemic stroke is a disease of the brain that can lead to disability and death in adults. In 85% of stroke cases, survivors suffer from long-term disability, such as movement and sensory disorders and impairment of learning and memory ability due to a variety of factors, such as blood-brain barrier (BBB) disruption, excitotoxic cell death, and edema formation (1,2). Ischemic stroke mainly involves occlusion of the middle cerebral artery (MCA), which provides sensory and motor areas with oxygen and nutrients. The therapeutic window for treating acute ischemic stroke is within 6 h (3), so our study focused on ischemic stroke during convalescence. Researchers have attempted to use a middle cerebral artery occlusion (MCAO) model to investigate the timing of BBB repair under pathological conditions, but an agreement on whether two or three weeks are needed has yet to be reached (4,5). Regardless of the duration of BBB repair, obvious cerebral ischemia/reperfusion injury can be observed after 24 to 72 h (6).

The BBB is a complex structure that is mainly composed of endothelial cells, pericytes, astrocytic foot processes, basement membrane and tight junctions (TJs) (7). An intact BBB under physiological conditions and a repaired BBB under pathological conditions prevent the entry of peripheral inflammatory substances and regulate the exchange of toxins and nutrients between the brain and blood (8). However, the BBB is an obstacle to the transport of large molecules into the brain, including those used for the treatment of CNS diseases such as stroke and Alzheimer's disease (AD) (9). Many experimental research studies have aimed to disrupt or bypass the BBB to deliver therapeutic drugs using, for example, focused ultrasound, mannitol, intranasal delivery and intraventricular injection (10-12), but these methods are difficult to apply in the clinic. Therefore, the exploration of practical methods that safely, effectively, noninvasively, and repeatedly promote the permeability of the BBB to facilitate drug delivery to the brain is both crucial and of significant clinical interest (13-14).

The stimulation parameters of electronic acupuncture (EA), a modern and widely accepted therapy for stroke, can be easily and clearly controlled (15-16). Moreover, our previous study demonstrated that EA stimulation can open the BBB of rats with cerebral ischemia reperfusion induced by contusion while not inducing obvious brain edema (17). In a recent systematic review, the therapeutic effect of Baihui (GV20)-based scalp acupuncture was confirmed in animal models of focal cerebral ischemia (18). Another study indicated that multiple applications of EA at GV20 and Shuigou (GV26) could significantly alleviate cerebral infarction and enhance the sensorimotor ability of ischemic rats (19). According to traditional Chinese medicine (TCM), because GV20 and GV26 are both on the "Du meridian", they govern blood vessels. Recent studies have attempted to clarify the ability of EA stimulation at GV20 and GV26 to increase cerebral blood flow and improve cerebral vascular circulation (20-21). The acupuncture points, approach and parameters of EA can be adjusted to exert different effects on the CNS. Therefore, EA may be a reliable and effective method for treating CNS diseases such as stroke in the clinic (22).

Nerve growth factor (NGF), the first neurotrophic drug to be discovered, plays an active role in regulating neuronal development, differentiation, plasticity, cell death and survival (23). However, the molecular weight of NGF is approximately 13.4 kDa, making it difficult to cross the BBB under normal conditions and reach its effective drug concentration to exert its therapeutic effect (24). Thus, we believe that EA at GV20 and GV26 can be used to open the BBB and facilitate the entry of drugs such as NGF into the brain to treat CNS diseases. Our previous study showed that the dilatational waves delivered through EA at GV20 and GV26 can promote the passage of Evans blue (EB) through the BBB, indicating that similar passage of NGF through the BBB may be possible (25). Subsequently, we conducted a preliminary study on the ability of EA to open the BBB with fluorescein isothiocyanate-dextran (FITC-dextran) as a tracer. Later, we found that 20 kDa FITC-dextran, which has a molecular similar to that of NGF, can also be induced to pass through the BBB via EA (data not shown). Inspired by these findings, we labeled NGF with FITC to allow visual observation of its entry into the brain.

Therefore, in this study, the effect of EA on facilitating the passage of NGF through the BBB and its influence on learning and memory in MCAO/R rats were assessed. These experiments were conducted in three parts. First, we determined the duration of BBB repair after MCAO. Second, based on the first

experiment, EA was used with specific parameters to preliminarily explore its ability to induce NGF passage through the BBB and to clearly determine whether NGF is taken up by neurons. Finally, we assessed the therapeutic effects of NGF on learning and memory in MCAO/R rats under EA stimulation to provide a theoretical basis for the use of EA to induce the entry of CNS-targeting drugs through the BBB for the treatment of ischemic stroke.

Materials And Methods

Animals

Adult male Sprague-Dawley (SD) rats (3 months old) weighing 250–270 g were obtained from Zhejiang Chinese Medical University. All mice were kept on a 12-h light/dark cycle and provided ad libitum access to food and water. All procedures in this study were performed in compliance with the National Institutes of Health Guide for Care and Use of Laboratory Animals. All efforts were made to alleviate animal suffering, minimize the number of animals used, and utilize alternatives to in vivo techniques when possible.

Establishment Of The Mcao Model

The rats were subjected to MCAO using an intraluminal thread according to a previously described method with some modifications. Briefly, the rats were allowed free access to water and then anesthetized with sodium pentobarbital (50 mg/kg) intraperitoneally (i.p.). The right common carotid artery (CCA), external carotid artery (ECA) and internal carotid artery (ICA) were carefully exposed and isolated from the vagus nerve under sterile conditions. The MCA was occluded by inserting a thread into the ICA through the CCA stump and advancing it until it blocked the origin of the MCA. Body temperature was monitored and maintained at 36.5–37.5°C throughout the surgery with an infrared heat lamp and a heating pad. After 90 min of ischemia, the suture was carefully withdrawn to induce reperfusion. After they recovered from anesthesia, the rats were returned to their cages and provided access to food and water ad libitum.

Neurological Deficit Test

Neurological deficit scores were determined by an examiner who was blinded to the group assignments 24 h after MCAO. A modified scoring system was used for this evaluation as follows: 0, no apparent neurological deficits (normal); 1, inability to extend the left forepaw when lifting the tail (mild deficit); 2, mild circling to the contralateral side when walking (moderate deficit); 3, slumping toward the contralateral (paralyzed) side (severe deficit); and 4, inability to walk autonomously without loss of consciousness (very severe deficit). MCAO was considered to be successfully induced in rats with a neurological deficit score of 1 to 3. In this study, rats that died from pulmonary insufficiency or subarachnoid hemorrhage and asphyxia were eliminated.

Experiment 1

Male SD rats were randomly divided into the following five groups (n=13 rats each): the control group; the MCAO-24 hour group; the MCAO-72 hour group; the MCAO-2 week group; and the MCAO-3 week group. Each group was further randomly divided into three subgroups (A, B, and C), and the cerebral infarction volume, ultrastructural changes in the BBB and permeability of the BBB were assessed. The rats in the MCAO groups underwent the MCAO-induction operation, while the control group did not. The cerebral infarction volume was measured in the rats in the A subgroups (n=5 rats each). Ultrastructural changes in the BBB were observed using transmission electron microscopy in the rats in the B subgroups (n=3 rats each). The permeability of the BBB was examined in the rats in the C subgroups (n=5 rats each) after injection with 2% EB in saline via the caudal vein using an indwelling needle (4 ml/kg).

Ttc Staining

2,3,5-triphenyltetrazolium chloride (TTC, T8170, Solarbio, Beijing) staining was exploited to assess the infarct volume. Briefly, rats were deeply anesthetized with sodium pentobarbital intraperitoneally and sacrificed by decapitation at the appropriate time point. The brains were rapidly dissected and sectioned into five coronal slices with an approximate thickness of 2 mm; these slices were then stained for 20 min at 37°C with 2% TTC, coloring the noninfarcted areas in slices red, while the ischemic area remained colorless. By dividing the total infarct volume by the volume of the whole brain area, the infarct volume percentage was calculated with ImageJ software.

Blood-brain Barrier Ultrastructure

The rats were anesthetized with sodium pentobarbital intraperitoneally, and the tissues of the ischemic penumbra (1.0 mm × 1.0 mm × 1.0 mm) were perfusion-fixed with 2.5% glutaraldehyde at the appropriate time point. The brain tissues were maintained at 4°C for 2–4 h and washed in 0.01 M phosphate-buffered saline (PBS) three times. After rinsing, the samples were postfixed in 1% osmium tetroxide, washed in 0.1 M PBS three times and dehydrated in a graded ethanol series (50–100%). The samples were embedded in epoxy resin (Epon 812) and stained with methylene blue. Ultrathin sections (70 nm) were cut on an ultramicrotome (HM335E; Microm GmbH, Waldorf, Germany) and stained with uranyl acetate and lead citrate. The sections were then imaged with a transmission electron microscope (H-7650; Hitachi, Ltd., Tokyo, Japan).

Assessment Of Eb Permeability Under Laser Confocal Microscopy

The brains of the rats in the C subgroups were sectioned into 30 μm slices after EB quantification. Then, five slices of the prefrontal lobe were selected at intervals of 3 mm and placed under a laser confocal

microscope (LCM, Nikon Eclipse Ti). Red light was applied, and photographs were taken with a laser confocal microscope in the Cy5 channel. The images were processed using NIS-elements AR and Adobe Photoshop.

EB quantification with a small animal physiological signal telemetry device

The brains of rats in the C subgroups were placed in a small animal physiological signal telemetry device (IVIS Lumina LT, PerkinElmer, USA). The Cy5.5 channel was used, and ovals of the same size were drawn. Then, the mean fluorescence intensity with the ovals was measured to reflect the deposition of EB in the brain tissue.

Experiment 2

The group in which the BBB was basically repaired based on experiment 1 was further used as the MCAO/R model group (3 weeks after MCAO operation). These MCAO/R rats were randomly divided into the MCAO model group and the MCAO model-EA group. Additionally, a control group and control-EA group were included (n=10 rats each). Acupuncture needles (length 25 mm, diameter 0.30 mm; Hwato, Suzhou Medical Supplies Factory Co, Ltd, China) were inserted at GV20 (Baihui) and GV26 (Shuigou) in the rats in the EA groups. The needles were then connected to an acupuncture point nerve stimulator (HANS-200, Nanjing Jinsheng, Ltd, China), and stimulation with a frequency of 2/100 Hz and an intensity of 2 mA was administered for 40 min (a homemade relay cycled power to the electrode for 6 sec on and 6 sec off). Each group was further randomly divided into two subgroups (n=5 rats each) based on the drug (NGF solution or FITC-NGF solution) injected into the caudal vein. The rats in the A subgroups were injected with NGF in PBS (10 μg/kg), while the rats in the B subgroups were injected with FITC-NGF in PBS (10 μg/kg). The degree of NGF penetration was assessed using a spectrophotometer, while FITC-NGF penetration was evaluating using laser confocal microscopy and a digital pathologic section (fluorescence) scanning analyzer.

NGF ELISA

NGF solution (XF8415011, R&D Systems, 10 μg/kg) was injected into the caudal vein of the rats. After injection, the rats in the control group and the MCAO/R model group were allowed to rest for 30 min, while the rats in the EA groups were immediately treated with EA and then allowed to rest. Then, the rats were deeply anesthetized and perfused with PBS. Their brains were obtained, and the right cerebral cortex was weighed. After homogenization, the brains were centrifuged at 18000 rpm for 30 min at 0°C. The supernatant was collected, and the concentration of NGF was measured using an Ab100757 β-NGF Rat ELISA Kit (GR212598-1, Abcam, USA) according to the manufacturer's instructions. A multifunctional microplate reader (SpectraMax M5, Molecular Devices Co, USA) was used to measure NGF content.

Synthesis Of Fitc-ngf Conjugate

A 0.15 mol/L NaCl solution was prepared and mixed with a molar amount of NaHCO3-Na2CO3 solution (9:1, v/v). Then, murine β-NGF (96-450-34-100, PeproTech, USA) was dissolved in the solution (10 mg/ml), which was then stored at 4°C. In the dark, FITC (F7250-50, Sigma-Aldrich, USA) was dissolved in NGF-containing solution (50-50 mg: 1 mg, M/M), which was then stirred with an electromagnetic stirrer for 14 h at 4°C. Sephadex was used to separate the FITC and FITC-NGF in the mixture. The obtained FITC-NGF conjugate was freeze-dried and stored under sealed conditions in the dark for further use.

Immunofluorescence Staining

Immunofluorescence analyses were performed according to standard protocols. Briefly, the brains were isolated and postfixed in 4% PFA overnight at 4°C before being preserved in 30% sucrose in PBS. Then, the brains were coronally sectioned into 30 μm slices with a Leica CM1950 cryostat. Five equally spaced slices of the prefrontal lobe of each brain were then selected to evaluate the penetration of FITC-NGF into the blood vessels, while another 5 slices were selected to observe the uptake of FITC-NGF by neurons. Next, the slices were washed in PBS once and blocked in blocking buffer (0.3% Triton+5% goat serum in PBS or 0.3% Triton+ 10% donkey in PBS solution) in a 37°C water bath incubator for 1 h. The slices were then incubated with the following primary antibodies at 4°C overnight: rabbit anti-laminin (1:200, Abcam, ab11575) and anti-NeuN (1:600, Abcam, ab104224). After being washed 3 times in PBS, the brain slices were incubated in goat anti-rabbit IgG H&L (HRP) secondary antibody (1:400, Abcam, ab205718) diluted in PBS containing 5% goat serum or in Alexa Fluor 647-conjugated AffiniPure donkey anti-mouse IgG (1:800, Jackson ImmunoResearch, 715-605-150) diluted in PBS containing 10% donkey serum at 37℃ in a constant temperature water bath for 1 h. After incubation, the brain slices were washed, dried, and mounted with Fluoroshield Mounting Medium with DAPI. The brain slices were observed under a laser confocal microscope with the Cy5 channel and the FITC channel in the dark. The images were processed using NIS-elements AR and Adobe Photoshop. The uptake of FITC-NGF by neurons was calculated by determining the mean positive cell rate in the 5 slices from each rat.

Quantification of FITC-NGF by a digital pathology section (fluorescence) scanning analyzer

FITC-NGF signal was observed in frozen 30 μm-thick brain slices using a digital pathological section (fluorescence) scanning analyzer, and the green fluorescence integrated optical density (FIOD) values of FITC-NGF in the cerebral cortex were measured using Image-Pro Plus software 6.0 and statistically analyzed (FIOD/area ∗100) as a measure of the deposition of FITC-NGF. The mean FIOD value was used to reflect FITC-NGF expression in the prefrontal lobe in 5 equally spaced slices from each rat.

Experiment 3

Based on the results of experiment 2, the frequency for delivering electronic acupuncture was determined. The MCAO/R rats (3 weeks after MCAO operation) were randomly divided into the MCAO model group, the MCAO model-NGF group, the MCAO model-EA group and the MCAO model-EA-NGF group; a control

group was also included (n=5 rats each). The rats in the MCAO model-NGF group and MCAO model-EA-NGF group were injected with NGF (2018070423005, Hiteck, China) solution (10 μg/kg) once a day for six days, and the rats in the MCAO model group and MCAO model-EA group were injected with the same volume of saline solution into the caudal vein. After each injection, the EA groups underwent treatment with acupuncture needles and an acupuncture point nerve stimulator (2/100 Hz, 2 mA, 40 min, 6 sec on/6 sec off), while the other groups were restrained but did not receive any EA treatment. Before each injection, the rats were subjected to the Morris water maze to assess learning and memory. On the sixth day after injection or EA stimulation, the rats were allowed to rest for 30 min and then decapitated. The brains were removed, and neuronal apoptosis was measured by TUNEL staining.

Analysis of spatial learning and memory with the Morris water maze

Male SD rats were trained on the Morris water maze to assess their spatial learning and memory. The water maze consisted of a circular pool measuring 180 cm in diameter and was surrounded by 70 cm-high walls. The depth of the pool was 50 cm, and the water temperature was 23°C ±1°C. A 12 cm-diameter platform was positioned 2 cm beneath the water surface. The SMART 3.0 (Panlab, Spain) system was used to record training trials, with the settings reflecting the fact that the SD rats were white and the walls and bottom of the pool were black. Four different shapes of yellow fluorescent paper were placed on the walls to act as spatial cues.

Before the trial, the ability of the rats to swim to and climb onto the platform was evaluated. Rats that could not swim or only swam to but could not climb onto the platform were excluded. Next, the rats were randomly divided into groups.

In the learning phase of the experiment (days 1–5), each rat was placed individually on the platform for 30 sec. Then, for each of four trials they performed per day, the rats were placed in the tank at one of four entry points, i.e., north, south, east, or west, in turn. The entry point was different from the one used in the prior trial, but in any trial, the entry point could be the same for all rats. In each trial, the rats had 90 sec to reach the platform, on which they were allowed to stay for 30 sec. If a rat could not find the platform within the allowed time, it was guided to and placed onto the platform, and the time was recorded as 90 sec. After each trial, the rats were placed on the platform for 30 sec. On day 5, the results for each trial were recorded as a measure of spatial learning.

On day 6, a probe trial in which the platform was removed was conducted to assess spatial memory. During the probe trial, the rats were allowed to search for the platform for 90 sec. The SMART 3.0 system was used to record the number of times the rats crossed the former location of the platform and the swimming path.

Tunel Assay

On day 6, the rats were allowed to rest for 30 min after injection or EA stimulation, after which they were deeply anesthetized and perfused with PBS until the brains exhibited no irritating odor. The brains were then cut into 4 μm-thick coronal slices in a mold, placed in a tissue embedding box, and soaked in 75% alcohol for 24 h. Next, the slices were dehydrated in gradient ethanol solutions at 55°C and dried. The slices were then placed in xylene I for 5 min followed by xylene II for 5 min and hydrated in gradient alcohol solutions. The slices were covered with Proteinase K without DNase (provided by a kit), incubated in a 37°C incubator for 30 min and washed with PBS. TUNEL reaction solution (G3250, PROMEGA) was added dropwise to the slices, which were then incubated at 37°C in the dark for 1 h, washed with PBS, dried, and mounted. A digital pathological section (fluorescence) scanning analyzer (OLYMPUS, Japan) was used to assess the TUNEL staining results. The green FIOD values of TUNEL in the same area of the right hippocampus were determined using Image-Pro Plus software 6.0 and statistically analyzed (FIOD/area $*$ 100).

Statistical Analysis

Data are plotted in graphs as the means ± standard errors of the mean (SEMs). Statistical analyses were carried out using IBM SPSS 20.0. For normally distributed measurements, the unpaired Student's t-test was used for comparisons between two groups, and one-way ANOVA followed by Tukey's post hoc test was used for comparisons among ≥3 groups. For measurements that are not normally distributed, the nonparametric Mann-Whitney U test between and Kruskal-Wallis test were used to perform comparisons between two groups and among three or more groups, respectively. Comparisons were considered significantly different if the p-value < 0.05.

Results

The Cerebral Infarction Volume Changed Over Time After Mcao

After MCAO, extensive lesions developed in the lateral cortices of the rats. Figure 1A and 1B show that in the MCAO groups, cerebral infarctions of varying degrees occurred in the region of the brain to which the middle cerebral artery supplies blood and its vicinity. Normal tissue stained deep red, while the infarct area appeared white. Figure 1B shows that in the MCAO groups, the volume of the cerebral infarctions was higher than that in the control group ($p < 0.01$). Compared with that in the 24 h group, 72 h group, and 2 w group, the volume of the cerebral infarctions in the 3 w group was significantly lower ($p < 0.01$). Analysis of the differences in the volume of the cerebral infarctions suggested that after MCAO, the brains of the rats in the 24 h group and 72 h group exhibited the highest degree of cerebral ischemia, while the brain tissue in the ischemic penumbra was in the process of repair in the 2 w group and 3 w group.

The Bbb Was Essentially Repaired Three Weeks After Mcao

We also examined changes in the BBB ultrastructure and EB permeability. As shown in Figure 1C, transmission electron microscopy revealed that in rats in the control group, the vascular lumen was normal in size and shape, and the vascular endothelial cells were smooth, not swollen, and closely arranged. Additionally, the basement membrane (BM) was intact and continuous. The nuclei were normal in size and shape, and the structure of the mitochondria and endoplasmic reticulum was intact. In the 24 h group, 72 h group and 2 w group, edema and "vacuolization" could be seen around the vascular endothelial cells, and the BM was incomplete or discontinuous. The nuclei were hyperchromatic, and some mitochondria were swollen. However, in the 3 w group, the shape of the vascular lumen was basically restored, and the thickness of the cell membrane was essentially normal. Compared with that of the other groups, these edema around the cells was significantly reduced in the 3 w group. Additionally, the BM and the nuclear structure were basically intact, the perinuclear space was uniform, and mitochondrial damage was minimal. To determine the permeability of the BBB, we use EB as a tracer. As shown in Figure 2A, under laser confocal microscopy, fluorescence imaging revealed that in the control group, EB was barely visible through the blood vessels in either cortical hemisphere. In the rats in the MCAO groups, EB was not observed to penetrate the blood vessels on the left side (nonischemic side), similar to the control group. On the right side (ischemia-penumbra), however, transport of EB across the BBB, as evidenced by a "lantern"-shaped pattern, could be seen in the 24 h group, 72 h group, and 2 w group but not the control group. However, in the rats in the 3 w group, this change in vascular permeability of the right ischemic penumbra was not obvious. To calculate the fluorescence intensity of EB in the rat cerebral cortex, a small animal physiological signal telemetry device was used. The heat map revealed that the fluorescence intensity in the control group was lower than that in the 24 h group and 72 h group ($p < 0.01$), as shown in Figure 2B and 3C. Compared with that in the 3 w group, the mean fluorescence intensity in the 24 h group and 72 h group was higher, and the difference was statistically significant ($p < 0.01$). Although the fluorescence intensity in the 3 w group was higher than that in the control group, the difference was not significant ($p > 0.05$). These results suggest that the BBB was basically repaired and that its function was restored, allowing it to prevent macromolecules from freely entering and leaving the brain three weeks after MCAO.

Ea Stimulation At A Specific Frequency Enhanced Bbb Permeability

We determined the specific frequency at which EA induced the most robust enhancement of BBB permeability by measuring the level of NGF and FITC-NGF penetration into the rat prefrontal cortex after EA stimulation. Figure 3A shows that NGF penetration in the control-EA group was higher than that in the control group, but the difference was not significant ($p > 0.05$); additionally, compared with that in the model group, NGF penetration was increased in the model-EA group ($p < 0.01$). As shown in Figure 3B and 3C, examination of FITC-NGF content showed that FITC-NGF penetration in the control-EA group was significantly higher than that in the control group ($p < 0.01$) and that FITC-NGF penetration in the model-EA group was also higher than that in the model group ($p < 0.01$). The differences in NGF and FITC-NGF

content in the prefrontal cortex suggest that EA stimulation at a specific frequency enhanced BBB permeability.

EA stimulation induced FITC-NGF uptake by prefrontal neurons through blood vessels

After identifying the specific frequency at which EA had the most robust effect on BBB permeability, we used EA at this frequency to assess the passage of FITC-NGF through the BBB. As shown in the fluorescence images of brain tissue sections in Figure 4, FITC-NGF showed lantern-like infiltration of the blood vessels in the control-EA group and model-EA group but not in the control group or model group. After evaluating FITC-NGF penetration through the blood vessels, we speculated that it could be taken up by neurons. Therefore, we obtained fluorescence images to assess FITC-NGF uptake. As shown in Figure 5A and 5B, more neuronal FITC-NGF uptake was observed in the control-EA group than in the control group in the prefrontal cortex ($p < 0.05$). The FITC-NGF content in the model-EA group was significantly higher than that in the model group, and the difference was statistically significant ($p < 0.01$). Therefore, EA stimulation promoted the passage of NGF and FITC-NGF through the BBB, and NGF could be taken up by neurons.

Induction of NGF entry into the brain by EA promoted learning and memory in rats and inhibited apoptosis of neurons in the hippocampus

EA stimulation can enhance BBB permeability, facilitating the uptake of NGF by neurons by allowing it to pass through the BBB. Therefore, we further investigated the effects of NGF entry into brain tissue. Figures 6 and 7 show changes in the learning and memory ability in the rats. The control group traveled a shorter distance and showed a shorter latency in finding the platform on day 5 than the model group and the model-NGF group ($p < 0.01$); however, this parameter was not significantly greater in the model-EA-NGF group than in the control group ($p > 0.05$). The latency in finding the platform in the model-EA-NGF group was significantly shorter than that in the model group and model-NGF group ($p < 0.01$), but the difference with that in the model-EA group was not significant ($p > 0.05$). In the probe trial on day 6 in figure7, the model-EA-NGF group crossed the target quadrant ($p < 0.01$) more times than the model group and model-EA group but not the control group ($p > 0.05$). Figure 8 shows that the level of apoptosis in the model-EA-NGF group was significantly smaller than that in the model group, model-NGF group and model-EA group ($p < 0.01$), as determined by analysis with the DeadEnd TM Fluorometric TUNEL Kit. We also obtained fluorescence images of the right hippocampal region and found that TUNEL staining was very low in the control group. These results suggest that upon EA stimulation increasing the permeability of the BBB, NGF entered the brain to exert its therapeutic effect, inhibit apoptosis in the hippocampus and promote learning and memory in rats.

Discussion

Ischemic stroke is a common clinical disease associated with high mortality and disability rates. Therefore, it is vital to establish an animal model of the disease and identify potential treatments to improve the quality of life of patients. The MCA is involved in ischemic stroke. The pathological process

initiated by occlusion of the MCA is similar to that of clinical stroke, and therefore this procedure is widely regarded as a standard method for inducing an animal model of focal cerebral ischemia. In this experiment, an MCAO/R model was established by using the Zea Longa method. Blood flow through the right MCA of rats was blocked and restored by inserting and removing an intraluminal thread, producing the MCAO/R model (26). In this model, blood flow can be restored in a timely manner under waking conditions, affecting the rats little. Thus, it can be used for research on the recovery process that occurs after brain injury.

In the acute stage after cerebral ischemia, i.e., from day 1 to day 3, BBB dysfunction first triggers cytotoxic edema within minutes followed by the onset of vasogenic edema associated with BBB breakdown (27). The results of our study showed that the volume of cerebral infarction at 24 h and 72 h was significantly increased and tended to be lower at 3 w. This is consistent with the results from another research group, who observed severe brain damage and high permeability 24 h and 72 h after cerebral ischemia. Although some research groups indicate that 2 weeks of recovery after an MCAO operation is sufficient, others support the hypothesis that the BBB is essentially repaired only after 3 weeks (28-29). Our findings can be explained by the fact that AQP4-dependent transcellular water flux is critical to the movement of edema fluid across the astrocyte cell membrane in the glia limitans into the CSF (30). In addition to inducing edema, cerebral ischemia also results in cellular reactions such as angiogenesis and the reconstruction of functional microvasculature to facilitate stroke recovery. VEGF and angiopoietins are crucial for angiogenesis and protection against ischemic injury (31), and the upregulation of VEGF expression not only promotes angiogenesis but also enhances microvascular permeability (32). Interestingly, we found that EB was barely visible in the control group and on the nonischemic side in the MCAO group because the BBB was still intact, allowing it to limit entry of the EB-albumin complex. Similarly, the 3-week group did not demonstrate EB penetration of blood vessels, indicating that the barrier function of the BBB may have been restored. The heat map of the fluorescence intensity obtained in our study also supports this hypothesis. We used transmission electron microscopy to visually assess BBB structure and function after inducing MCAO, observing signs of endothelial cell swelling, mitochondrial membrane structural damage and surrounding cavitation necrosis, which is in line with studies demonstrating that connexin channels are targets for manipulating endothelial calcium dynamics in the brain and BBB permeability (33). Furthermore, we observed fewer swollen mitochondria and relatively intact endothelial cell structures in the 3-week group. The pathological process here potentially involves salvaging tissue in the ischemic penumbra (34). A recent review of the literature revealed that following cerebral ischemia, vascular permeability is changed and the BBB is damaged, leading to brain edema, inflammation, neuronal necrosis and apoptosis (35). These outcomes are related to alterations in BBB ultrastructure and function (36). However, the data obtained in this study showed recovery of the BBB ultrastructure, limited passage of EB through the BBB and a decreased brain edema volume in the 3-week group, suggesting that the BBB was basically repaired three weeks after MCAO.

The BBB, a physical and metabolic barrier essential for maintaining CNS homeostasis and preventing potentially harmful circulating substances from entering the brain, mainly comprises brain endothelial cells, pericytes, astrocytes, microglia, neurons, and extracellular matrix components. However, due to its

low permeability, the BBB prevents drugs with molecular weights greater than 500 Da from entering the brain under physiological conditions (37). Hence, a safe and effective method for increasing the permeability of the BBB is urgently needed. Previous studies have demonstrated the effectiveness of EA in increasing the permeability of the BBB in rats recovering from MCAO (38). Current methods for opening the BBB include techniques based on ultrasound, hypertonic saline solutions and drugs. However, these opening methods have disadvantages, such as the generation of an inflammatory response, a short or uncontrollable opening time, and dose dependence (39,40). In contrast, EA stimulation increases the permeability of the BBB and can be regulated bidirectionally. Under physiological conditions, high-frequency EA can open the BBB to a certain extent while protecting the damaged BBB in pathological conditions (41). Therefore, we selected safe and controllable EA as a means of opening the BBB. Additionally, ELISA revealed that with specific parameters, EA stimulation increased the amount of exogenous NGF in the brain under physiological and pathological conditions but did not affect the physical structure of the BBB, which is important for preserving cellular integrity and the health of the brain and the CNS (42). To visually observe the passage of NGF across the BBB, we labeled the primary amine group of NGF with FITC, establishing a stable urea bond covalently to form FITC-NGF (43). In general, FITC-NGF emits yellow-green fluorescence that permits tracing of the bonded NGF. The results revealed that EA at a specific frequency can open the BBB and induce the entry of FITC-NGF into the brain. Because NGF binds to two types of membrane receptors, tropomyosin receptor kinase A (TrkA) and pan-neurotrophin receptor p75 (p75NTR) (44), we explored whether entry of exogenous NGF into the brain may be taken up by neurons. The findings agreed with our hypothesis; as anticipated, EA stimulation enhanced BBB permeability and induce NGF uptake by prefrontal neurons, suggesting a way for exogenous NGF to exert its neurotrophic effects in the CNS.

Increasing evidence has demonstrated that although it interacts with both receptors, NGF has a high affinity for TrkA and a low affinity for p75 (45). TrkA has a positive effect, maintaining neuronal survival and growth (46), whereas p75 often has a negative effect, such as inducing apoptosis (47); however, both are single transmembrane proteins on cells (48). More recent evidence confirmed that I^{125}-β-NGF is widely distributed in the basal forebrain, frontal cortex, hippocampus, cerebellum, and olfactory bulb in rats (49). The frontal cortex and the hippocampus have been studied extensively for their critical roles in spatial working memory. Additional experimental results indicated that the hippocampal network is the major brain network of working memory in rats (50). Therefore, we focused on the effect of NGF in the hippocampus because in patients, apoplexy sequelae are often accompanied by impaired contextual and spatial memory performance, which is tightly correlated with changes in the hippocampus (51). Our findings provide compelling evidence for the development of obvious cognitive impairment in rats after MCAO and the reversal of these impairments by EA stimulation and NGF entry into the brain. This result appears to be in agreement with recent papers showing that EA ameliorates cognitive impairment through inhibition of Ca^{2+}-mediated neurotoxicity in a rat model of cerebral ischemia-reperfusion injury (52). Other recent studies have demonstrated that it is feasible to attenuate cognitive impairment by reducing hippocampal neuronal degeneration and apoptosis (53). We hypothesized that under EA stimulation, NGF is able to enter the brain and exert its pharmacodynamic effect to promote learning and

memory by increasing the survival of neurons in the hippocampus and inhibiting apoptosis. The experimental results support this hypothesis, and all results indicate that the entry of NGF into the brain alleviated the impairment of cognitive function, which may be related to the inhibition of neuronal apoptosis in the hippocampus.

This study was an extension of our earlier study in which 2/100 Hz EA was applied to the GV20 and GV26 acupoints for 40 min, effectively increasing BBB permeability in rats. Initially, our research team was inspired by the basic theory of traditional Chinese medicine (TCM), in which the GV20 (Baihui) and GV26 (Shuigou) acupoints are situated on the head and face and refresh and calm the mind following stimulation. A recent study suggested that certain nerves and blood vessels, such as the greater occipital nerve and branch of the frontal nerve, are superficially and richly distributed beneath GV20, which plays a role in regulating blood circulation due to its effect on the CNS. Meanwhile, the second branch of the trigeminal nerve and the buccal branch of the facial nerve are distributed under the GV26, and stimulation of this acupoint can stimulate the trigeminal nerve and facial nerve, acting on the brainstem to promote respiratory rhythm, hypertension and other brain functions (54,55). Accordingly, we selected GV20 and GV26 as EA stimulation points and observed the effects on BBB permeability. According to previous experimental results, we preliminarily determined the parameters of EA stimulation required for stable opening of the BBB. We also found that enhancement of BBB permeability may be related to disruption of interendothelial TJs, causing the formation of gaps between endothelial cells resulting from the activation of neurons that release SP and a decline in ZO-1 and occludin expression (56). Therefore, we aimed to apply EA at currently used parameters to a pathological model such as the MCAO model to facilitate the entry of macromolecule drugs such as NGF into the brain and provide a new method for the treatment of CNS diseases. However, in the present study, the precise timing of the opening and closing of the BBB under EA stimulation was not determined. Additionally, the cumulative effect of specific parameters of EA on opening the BBB, the difference in brain region opening and the relationship between brain regions, such as the frontal cortex and hippocampus, will be the focus of our next research. Moreover, the specific frequency at which EA facilitates drug entry into the brain and whether the opening mechanism involves astrocytes, pericytes, enzymes, and diverse transport systems, such as P-glycoprotein (P-gp), require further research.

Conclusion

In conclusion, our results demonstrated that the BBB was basically repaired in rats 3 weeks after MCAO, which simulates the sequelae of cerebral ischemia in the clinic. For an intact BBB under physiological conditions and a repaired BBB under pathological conditions, methods to increase the permeability are vital to facilitate the entry of beneficial substances into the CNS. This paper showed that under EA stimulation at a specific frequency, NGF reached the rat brain through the BBB and was taken up by prefrontal cortex neurons, allowing it to exert its pharmacological effects. More critically, we showed that entry of NGF into the brain by EA stimulation at a specific frequency improved the learning and memory ability of rats and inhibited the apoptosis of neurons in the hippocampus, providing a new method for treating central nervous system diseases with macromolecule drugs.

Declarations

Acknowledgements

This study was supported by the National Natural Science Foundation of China (no. 81774407).

Data availability statement

The raw data supporting the conclusions of this article will be made available by the authors, without undue reservation.

Ethics declarations

The animal study was reviewed and approved by the Institutional Animal Care and Use Committee of Zhejiang Chinese Medical University.

Author contribution

YBZ, and XL conceived and designed the experiments. PG, SZ,and XM performed the experiments. HW and LG analyzed the data. YBZ drafted the manuscript. XL revised the manuscript. All authors contributed to the article and approved the submitted version.

Competing interests

The other authors declare no competing interests.

References

1. Onwuekwe I, Ezeala-Adikaibe B. Ischemic stroke and neuroprotection. Ann Med Health Sci Res. 2012 Jul;2(2):186-90. doi: 10.4103/2141-9248.105669. PMID: 23439855; PMCID: PMC3573516.

2. Malik R., Dichgans M. Challenges and opportunities in stroke genetics. Cardiovasc. Res. 2018;114:1226–1240. doi: 10.1093/cvr/cvy068.

3. Cheripelli, B. K., Huang, X., McVerry, F., & Muir, K. W. (2016). What is the relationship among penumbra volume, collaterals, and time since onset in the first 6 h after acute ischemic stroke?. International journal of stroke : official journal of the International Stroke Society, 11(3), 338–346. https://doi.org/10.1177/1747493015620807.

4. Chen, L. B. L. X. J. (2008). Study on the permeability of nerve growth factor through blood brain barrier after traumatic brain injury in rats. Chinese Journal of Neurosurgical Disease Research(03), 216-219.

5. Liu, M. (2019). Effects of Panax notoginseng Saponins on Ultrastructure of Neurovascular Units in Rats with Cerebral. Genomics and Applied Biology, 38(05), 2375-2381.

6. Zhang M, Lu H, Xie X, Shen H, Li X, Zhang Y, et al. TMEM175 mediates Lysosomal function and participates in neuronal injury induced by cerebral ischemia-reperfusion. Mol Brain. 2020;13(1):113. Published 2020 Aug 15. doi:10.1186/s13041-020-00651-z.

7. Małkiewicz MA, Szarmach A, Sabisz A, Cubała WJ, Szurowska E, Winklewski PJ. Blood-brain barrier permeability and physical exercise. J Neuroinflammation. 2019;16(1):15. Published 2019 Jan 24. doi:10.1186/s12974-019-1403-x.

8. Saili KS, Zurlinden TJ, Schwab AJ, Silvin A, Baker NC, Hunter ES 3rd, et al. Blood-brain barrier development: Systems modeling and predictive toxicology. Birth Defects Res. 2017;109(20):1680-1710. doi:10.1002/bdr2.1180.

9. Montagne A, Zhao Z, Zlokovic BV. Alzheimer's disease: A matter of blood-brain barrier dysfunction?. J Exp Med. 2017;214(11):3151-3169. doi:10.1084/jem.20171406.

10. Dauba A, Delalande A, Kamimura HAS, Conti A, Larrat B, Tsapis N, et al. Recent Advances on Ultrasound Contrast Agents for Blood-Brain Barrier Opening with Focused Ultrasound. Pharmaceutics. 2020;12(11):1125. Published 2020 Nov 21. doi:10.3390/pharmaceutics12111125.

11. Luo H, Shusta EV. Blood-Brain Barrier Modulation to Improve Glioma Drug Delivery. Pharmaceutics. 2020;12(11):1085. Published 2020 Nov 12. doi:10.3390/pharmaceutics12111085.

12. Islam SU, Shehzad A, Ahmed MB, Lee YS. Intranasal Delivery of Nanoformulations: A Potential Way of Treatment for Neurological Disorders. Molecules. 2020;25(8):1929. Published 2020 Apr 21. doi:10.3390/molecules25081929.

13. Stukas S, Robert J, Lee M, Kulic I, Carr M, Tourigny K, et al. Intravenously injected human apolipoprotein A-I rapidly enters the central nervous system via the choroid plexus. J Am Heart Assoc. 2014;3(6):e001156. Published 2014 Nov 12. doi:10.1161/JAHA.114.001156.

14. Konofagou EE. Optimization of the ultrasound-induced blood-brain barrier opening. Theranostics 2012;2:1223–37.6 Burgess A, Ayala-Grosso CA, Ganguly M, et al. Targeted delivery of neural stem cells to the brain using MRI-guided focused ultrasound to disrupt the blood-brain barrier. PLoS One 2011;6:e27877.

15. Tsui P, Leung MC. Comparison of the effectiveness between manual acupuncture and electro-acupuncture on patients with tennis elbow. Acupunct Electrother Res 2002;27:107–17.

16. Fang JF, Du JY, Shao XM, Fang JQ, Liu Z. Effect of Electroacupuncture on the NTS is modulated primarily by acupuncture point selection and stimulation frequency in normal rats. BMC Complement Altern Med. 2017 Mar 31;17(1):182. doi: 10.1186/s12906-017-1690-7. PMID: 28359336; PMCID: PMC5374564.

17. JS Zhang，H Zhou，YY Chen，Y Zhang，Y Song，JY Jiao, et al. Opening effect and regulation mechanism of rats'blood-brain barrier with electro-acupuncture treatment at Baihui (DU20) and Shuigou (DU26)points under different frequencies[J].China Journal of Traditional Chinese Medicine and Pharmacy,2018,33(05):2097-2102.

18. Wang WW, Xie CL, Lu L, Zheng GQ. A systematic review and meta-analysis of Baihui (GV20)-based scalp acupuncture in experimental ischemic stroke. Sci Rep. 2014 Feb 5;4:3981. doi: 10.1038/srep03981. PMID: 24496233; PMCID: PMC5379241.

19. Wang C, Yang F, Liu X, Liu M, Zheng Y, Guo J. Neurotrophic Signaling Factors in Brain Ischemia/Reperfusion Rats: Differential Modulation Pattern between Single-Time and Multiple Electroacupuncture Stimulation. Evid Based Complement Alternat Med. 2014;2014:625050. doi:10.1155/2014/625050.

20. Lv, Y., and He, Z. Research on the mechanism of "Xingnao Kaiqiao" at renzhong. J. Basic Chin. Med 2016. 22, 147–149.

21. Ran, M., Lihong, K., Fengjun, Q., Fengjun, Q., and Wei, M. Ancient and modern research on role of baihui to brain. Liaoning J. Traditional Chin. Med.46 2019, 425–428. doi: 10.13192/j.issn.1000-1719.2019.02.065.

22. Shih CC, Liao CC, Sun MF, Su YC, Wen CP, Morisky DE, et al. A Retrospective Cohort Study Comparing Stroke Recurrence Rate in Ischemic Stroke Patients With and Without Acupuncture Treatment. Medicine (Baltimore). 2015 Sep;94(39):e1572. doi: 10.1097/MD.0000000000001572. PMID: 26426630; PMCID: PMC4616848.

23. Valdovinos-Flores C, Limón-Pacheco JH, León-Rodríguez R, Petrosyan P, Garza-Lombó C, Gonsebatt ME. Systemic L-Buthionine -S-R-Sulfoximine Treatment Increases Plasma NGF and Upregulates L-cys/L-cys2 Transporter and γ-Glutamylcysteine Ligase mRNAs Through the NGF/TrkA/Akt/Nrf2 Pathway in the Striatum. Front Cell Neurosci. 2019;13:325. Published 2019 Jul 23. doi:10.3389/fncel.2019.00325.

24. Teleanu DM, Negut I, Grumezescu V, Grumezescu AM, Teleanu RI. Nanomaterials for Drug Delivery to the Central Nervous System. Nanomaterials (Basel). 2019;9(3):371. Published 2019 Mar 5. doi:10.3390/nano9030371.

25. YB Zhao, YY Chen, JS Zhang, XM Ling. Effects of different frequency of the electro-acupuncture on the opening of the blood-brain barrier of cerebral ischemia-reperfusion recovery rats[J].China Journal of Traditional Chinese Medicine and Pharmacy,2019,34(08):3422-3426.

26. Longa EZ, Weinstein PR, Carlson S, Cummins R. Reversible middle cerebral artery occlusion without craniectomy in rats. Stroke. 1989 Jan;20(1):84-91. doi: 10.1161/01.str.20.1.84. PMID: 2643202.

27. Dharmasaroja PA. Fluid Intake Related to Brain Edema in Acute Middle Cerebral Artery Infarction. Transl Stroke Res. 2016;7:49–53.

28. Stokum JA, Gerzanich V, Simard JM. Molecular pathophysiology of cerebral edema. J Cereb Blood Flow Metab. 2016;36:513–538.

29. Zhou L, Zhang J, Wang C, Sun Q. Tanshinone inhibits neuronal cell apoptosis and inflammatory response in cerebral infarction rat model. Int J Immunopathol Pharmacol. 2017;30(2):123-129. doi:10.1177/0394632017703274.

30. Papadopoulos M. C., Manley G. T., Krishna S., Verkman A. S. (2004). Aquaporin-4 facilitates reabsorption of excess fluid in vasogenic brain edema. FASEB J. 18, 1291–1293. 10.1096/fj.04-1723fje.

31. Michinaga S, Koyama Y. Pathogenesis of brain edema and investigation into anti-edema drugs. Int J Mol Sci. 2015;16(5):9949-9975. Published 2015 Apr 30. doi:10.3390/ijms16059949.

32. Zan L, Wu H, Jiang J, Zhao S, Song Y, Teng G, et al. Temporal profile of Src, SSeCKS, and angiogenic factors after focal cerebral ischemia: correlations with angiogenesis and cerebral edema.[J]. Neurochemistry International, 2011, 58(8):872-879.

33. De Bock M, Culot M, Wang N, Bol M, Decrock E, De Vuyst E, et al. Connexin channels provide a target to manipulate brain endothelial calcium dynamics and blood-brain barrier permeability. J Cereb Blood Flow Metab. 2011 Sep;31(9):1942-57. doi: 10.1038/jcbfm.2011.86. Epub 2011 Jun 8. PMID: 21654699; PMCID: PMC3185887.

34. Sharp FR, Lu A, Tang Y, Millhorn DE.Multiple molecular penumbras after focal cerebral ischemia. J Cereb Blood Flow Metab. 2000;20(7):1011-1032. doi: 10.1097/00004647-200007000-00001.

35. Pop, V., Sorensen, D. W., Kamper, J. E., Ajao, D. O., Murphy, M. P., Head, E, et al. (2013). Early brain injury alters the blood-brain barrier phenotype in parallel with β-amyloid and cognitive changes in adulthood. Journal of cerebral blood flow and metabolism : official journal of the International Society of Cerebral Blood Flow and Metabolism, 33(2), 205–214. https://doi.org/10.1038/jcbfm.2012.154.

36. Lin R, Yu K, Li X, Tao J, Lin Y, Zhao C, et al. Electroacupuncture ameliorates post-stroke learning and memory through minimizing ultrastructural brain damage and inhibiting the expression of MMP-2 and MMP-9 in cerebral ischemia-reperfusion injured rats. Mol Med Rep. 2016 Jul;14(1):225-33. doi: 10.3892/mmr.2016.5227. Epub 2016 May 9. PMID: 27177163; PMCID: PMC4918523.

37. Agundez J. A., Jimenez-Jimenez F. J., Alonso-Navarro H., Garcia-Martin E. (2014). Drug and xenobiotic biotransformation in the blood-brain barrier: a neglected issue. Front. Cell. Neurosci. 8:335. 10.3389/fncel.2014.00335.

38. J Zhang X Lin H Zhou Y Chen S Xiao J Jiao, et al. Electroacupuncture: a new approach to open the blood-brain barrier in rats recovering from middle cerebral artery occlusion. Acupunct Med.

2018;36(6):377-385. doi:10.1136/acupmed-2017-011496.

39. LeWitt, P. A., Lipsman, N., & Kordower, J. H. (2019). Focused ultrasound opening of the blood-brain barrier for treatment of Parkinson's disease. Movement disorders : official journal of the Movement Disorder Society, 34(9), 1274–1278. https://doi.org/10.1002/mds.27722.

40. Chu, C., Jablonska, A., Lesniak, W. G., Thomas, A. M., Lan, X., Linville, R. M, et al. (2020). Optimization of osmotic blood-brain barrier opening to enable intravital microscopy studies on drug delivery in mouse cortex. Journal of controlled release : official journal of the Controlled Release Society, 317, 312–321. https://doi.org/10.1016/j.jconrel.2019.11.019.

41. Tan Ke ping., Lin Xian-mirrg. (2007). Research and Development Tendency on Blood-Brain Barrier with Chinese Herbs and Acupuncture.Chinese Archives of Traditional Chinese Medicine, 2007, 25 (11):2283-2285.

42. Larsen J., Martin D., Byrne M. Recent Advances in Delivery Through the Blood-Brain Barrier. Curr. Top. Med. Chem. 2014;14:1148–1160. doi: 10.2174/1568026614666140329230311.

43. Le Guern F, Mussard V, Gaucher A, Rottman M, Prim D. Fluorescein Derivatives as Fluorescent Probes for pH Monitoring along Recent Biological Applications. Int J Mol Sci. 2020;21(23):9217. Published 2020 Dec 3. doi:10.3390/ijms21239217.

44. Delivanoglou N, Boziki M, Theotokis P, Kesidou E, Touloumi O, Dafi N, et al. Spatio-temporal expression profile of NGF and the two-receptor system, TrkA and p75NTR, in experimental autoimmune encephalomyelitis. J Neuroinflammation. 2020;17(1):41. Published 2020 Jan 29. doi:10.1186/s12974-020-1708-9.

45. Eibl JK, Strasser BC, Ross GM. Structural, biological, and pharmacological strategies for the inhibition of nerve growth factor. Neurochem Int. 2012;61:1266–1275.

46. Liebl DJ, Huang W, Young W, Parada LF. Regulation of Trk receptors following contusion of the rat spinal cord. Exp Neurol. 2001;167:15–26.

47. Zagrebelsky M, Holz A, Dechant G, Barde YA, Bonhoeffer T, Korte M. The p75 neurotrophin receptor negatively modulates dendrite complexity and spine density in hippocampal neurons. J Neurosci. 2005;25:9989–9999.

48. Song JN, Liu ZW, Sui L, Zhang BF, Zhao YL, Ma XD, et al. Dynamic expression of nerve growth factor and its receptor TrkA after subarachnoid hemorrhage in rat brain. Neural Regen Res. 2016;11(8):1278-1284. doi:10.4103/1673-5374.189193.

49. Zhou W, Zhang J, Wang G, Ling L, Yan C. Permeability and distribution of nerve growth factor in the brain of neonatal rats by periphery venous injection in hypoxic-ischemic state. Springerplus. 2016;5(1):1893. Published 2016 Oct 28. doi:10.1186/s40064-016-3594-2.

50. Griffin A. L. (2021). The nucleus reuniens orchestrates prefrontal-hippocampal synchrony during spatial working memory. Neuroscience and biobehavioral reviews, 128, 415-420. https://doi.org/10.1016/j.neubiorev.2021.05.033.

51. Cuartero MI, de la Parra J, Pérez-Ruiz A, Bravo-Ferrer I, Durán-Laforet V, García-Culebras A, et al. Abolition of aberrant neurogenesis ameliorates cognitive impairment after stroke in mice. J Clin Invest.2019;129(4):1536-1550.doi:10.1172/JCI120412.

52. Zhang Y, Mao X, Lin R, Li Z, Lin J. Electroacupuncture ameliorates cognitive impairment through inhibition of Ca^{2+}-mediated neurotoxicity in a rat model of cerebral ischaemia-reperfusion injury. Acupunct Med. 2018;36(6):401-407.doi:10.1136/acupmed-2016-011353.

53. Han B, Jiang W, Liu H, Wang J, Zheng K, Cui P, et al. Upregulation of neuronal PGC-1α ameliorates cognitive impairment induced by chronic cerebral hypoperfusion. Theranostics. 2020;10(6):2832-2848. Published 2020 Feb 3. doi:10.7150/thno.37119.

54. Yao BN. (2014). Clinical Study of moxibustion therapy in Baihui point on ischemic stroke. Modern Journal of Integrated Traditional Chinese and Western Medicine, 2014,23(13):1369-1371.

55. Wang, Y., & Yang, J. (2010). Zhongguo zhen jiu = Chinese acupuncture & moxibustion, 30(1), 23–26.

56. Zhang S, Gong P, Zhang J, Mao X, Zhao Y, Wang H, et al. Specific Frequency Electroacupuncture Stimulation Transiently Enhances the Permeability of the Blood-Brain Barrier and Induces Tight Junction Changes. Front Neurosci. 2020;14:582324. Published 2020 Oct 6. doi:10.3389/fnins.2020.582324.

Figures

Firgure 1

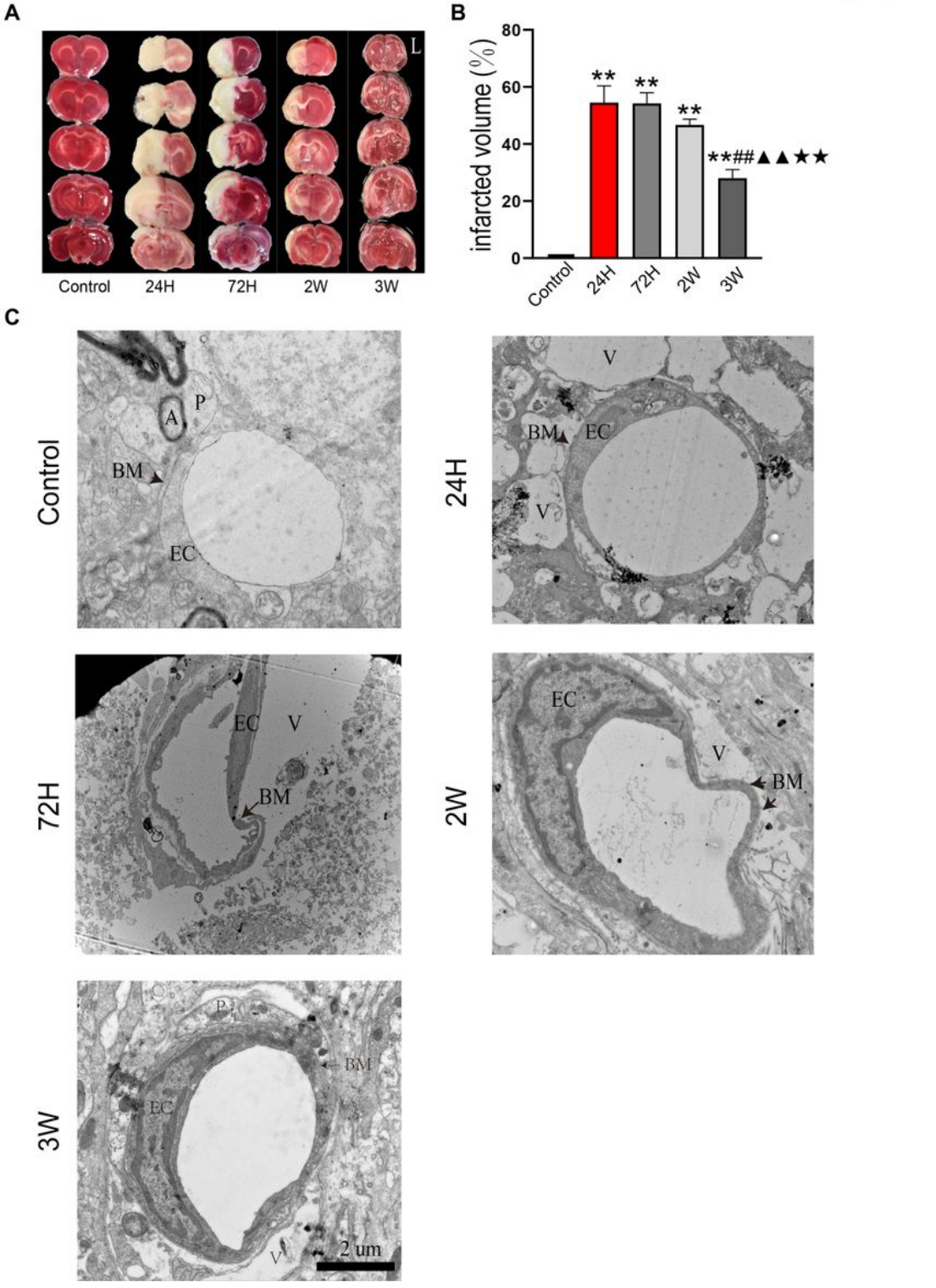

Figure 1

BBB repaired time after MCAO operation. (A) Representative images of brain sections stained with TTC. L, Left cerebral hemisphere. (B) Summary of cerebral infarct size in brain. The infarct volume was expressed as the percentage of the whole brain area. Data were expressed as mean ± SEM; **P <0.01, compared with control group; ##P <0.01, compared with 24H group; ▲▲P <0.01, compared with 72H group; ★★P <0.01 compared with 2W group; n = 5/group. (C) Changes in BBB ultrastructure in the control,

24H, 72H, 2W and 3W groups were observed by TEM; n = 3/group. A, astrocyte; BM, basal membrane; EC, endothelial cell; V, vacuole; P, pericyte.

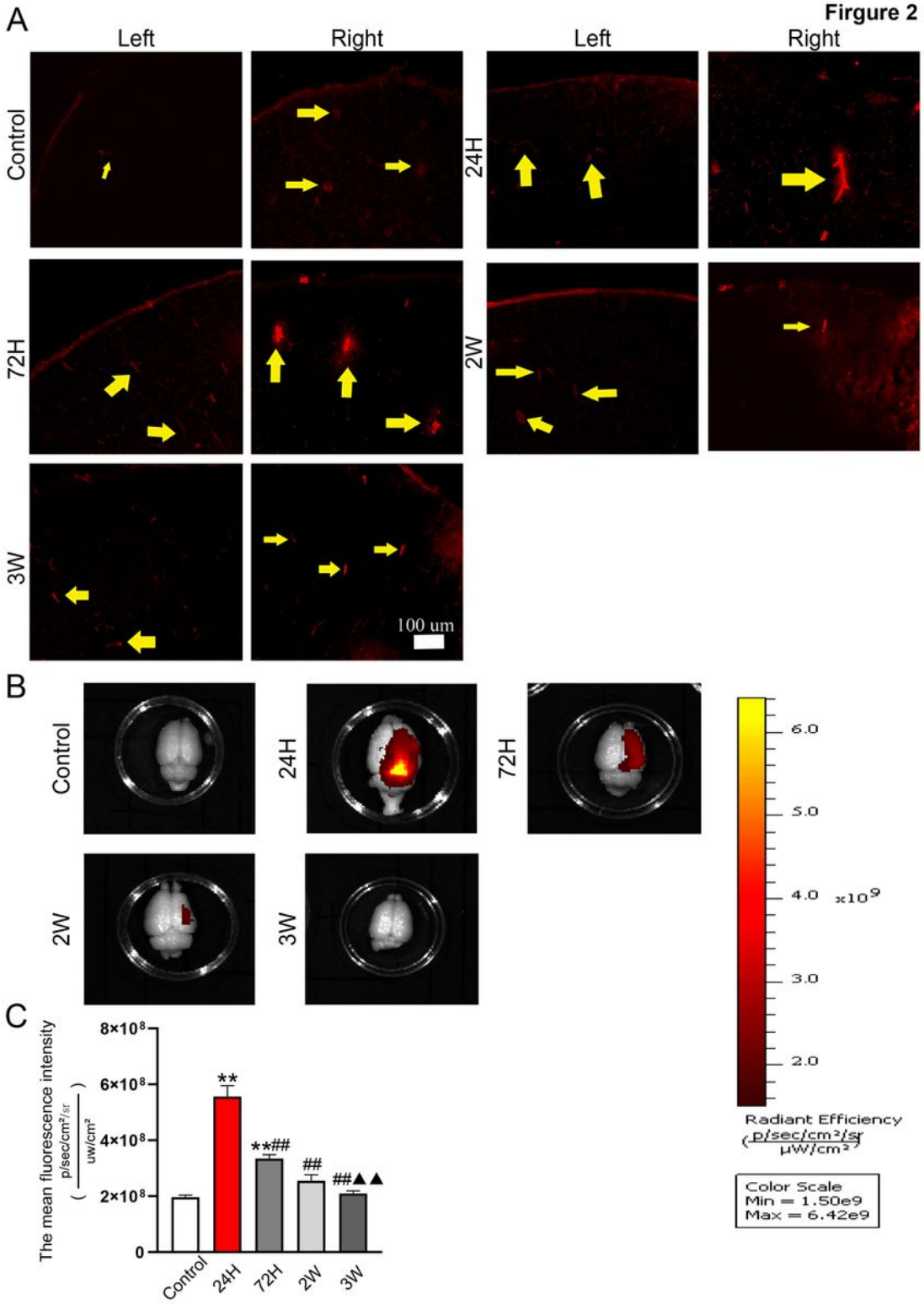

Figure 2

BBB repaired time after MCAO operation. (A) The permeability of the BBB in the control, 24H, 72H, 2W and 3W groups were observed under a fluorescence microscope, yellow arrows point to vessels. Focal ischemia is in right cerebral hemisphere. (B) In bioluminescent imaging of brains derived from rats

injected with EB in vein tail under a small animal physiologicalsignal telemetry device. Representative images are shown. (C) The mean fluorescence intensity was taken to reflect the deposition of EB in the brain tissue; **P <0.01, compared with control group; ##P <0.01, compared with 24H group; ▲▲P <0.01, compared with 72H group, n = 5/group.

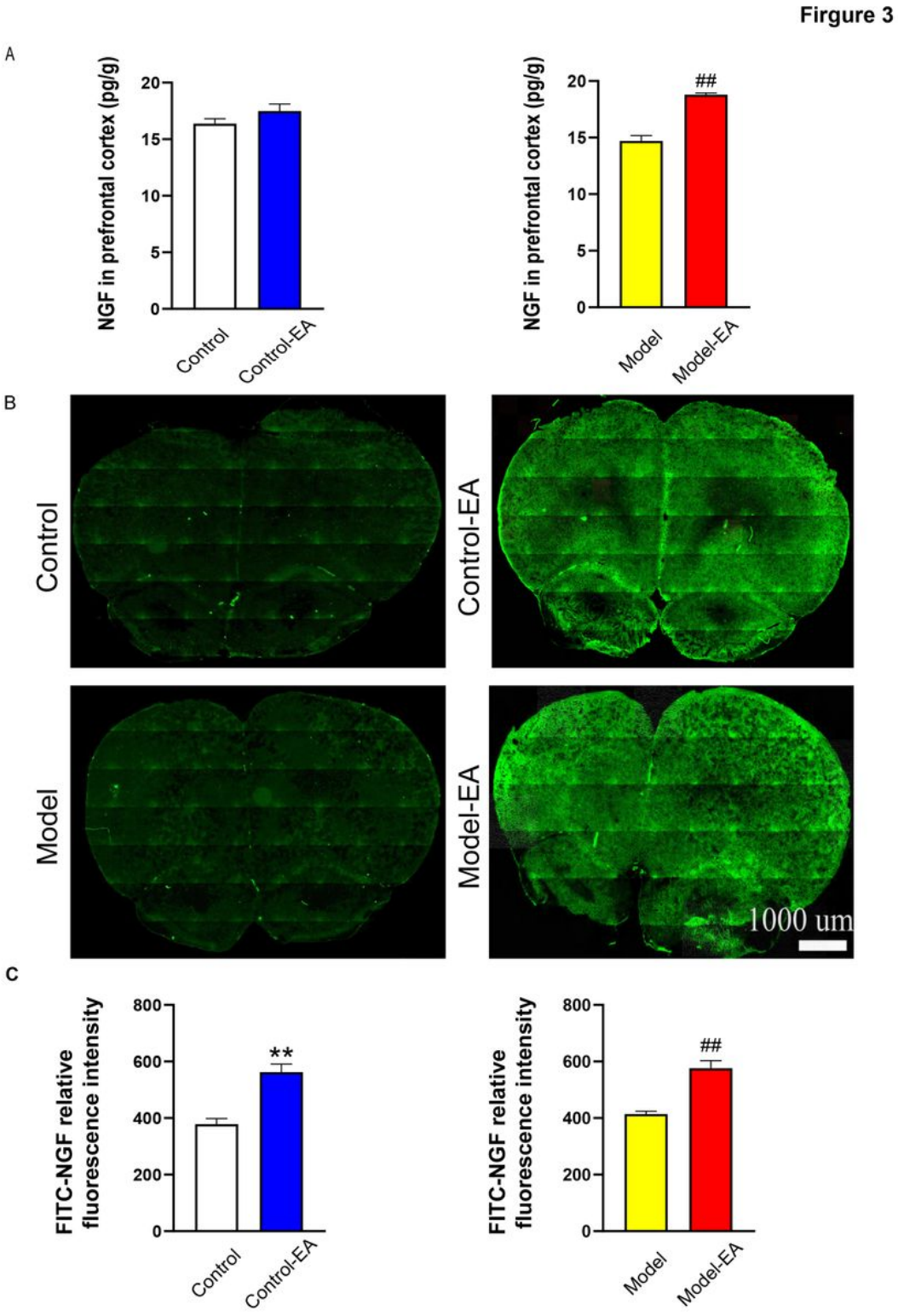

Figure 3

Specific frequency EA stimulation can induce NGF and FITC-NGF through BBB. (A) NGF content in the prefrontal cortex in the control, control-EA, model, model-EA group; P□0.05, control vs control-EA; ##P<0.01, model vs model-EA; n = 5/group. (B) The intensity and distribution of FITC-NGF fluorescence in coronal brain slices from each group. (C) FITC-NGF relative florescence intensity in each group; **P<0.01, control vs control-EA; ##P<0.01, model vs model-EA; n = 5/group.

Firgure 4

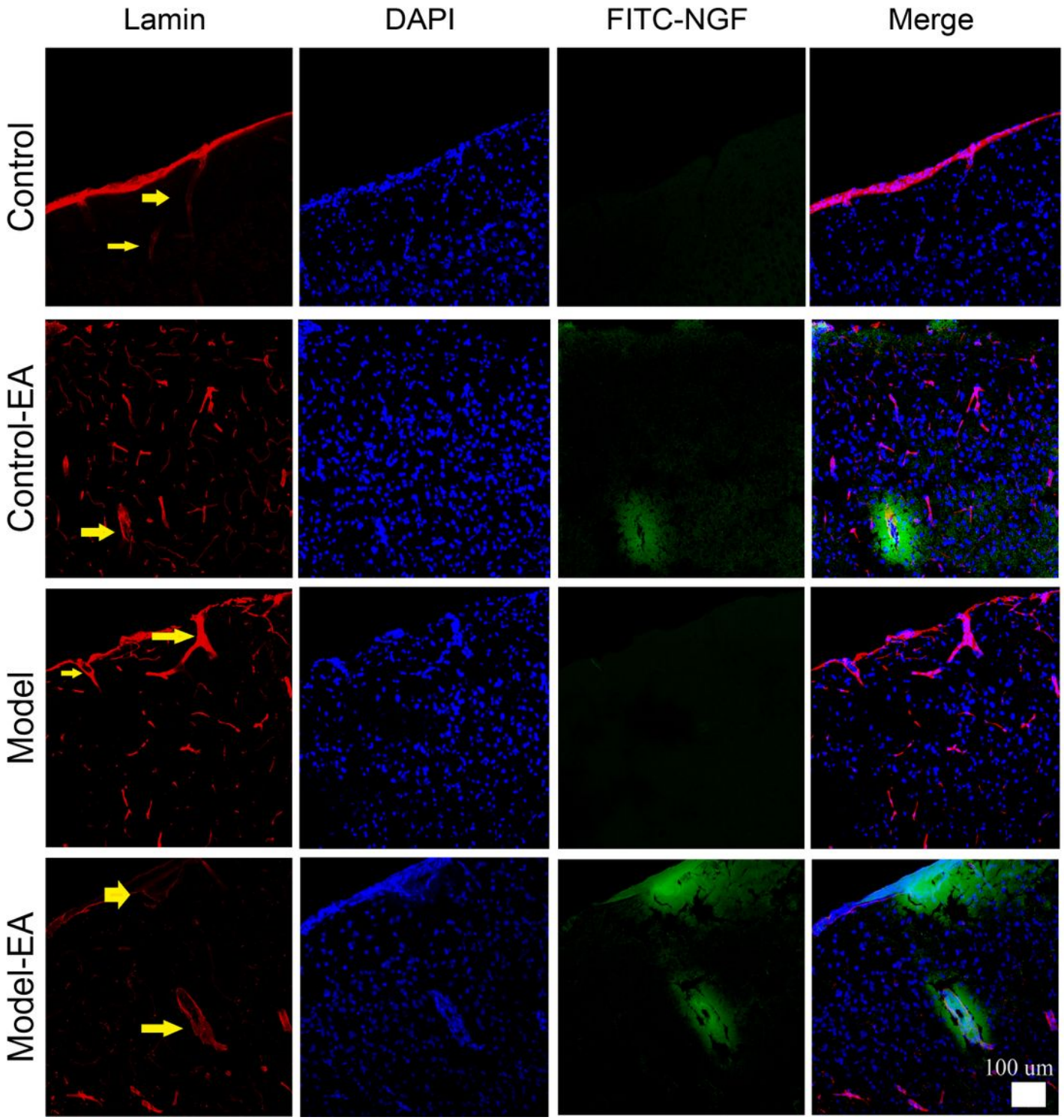

Figure 4

Specific Frequency EA Stimulation can open the BBB and facilitate FITC-NGF trough vessel. Fluorescence images showing that FITC-NGF diffused around the blood vessels in the control-EA group, and model-EA group in the prefrontal cortex, but control and model group had no such phenomenon.

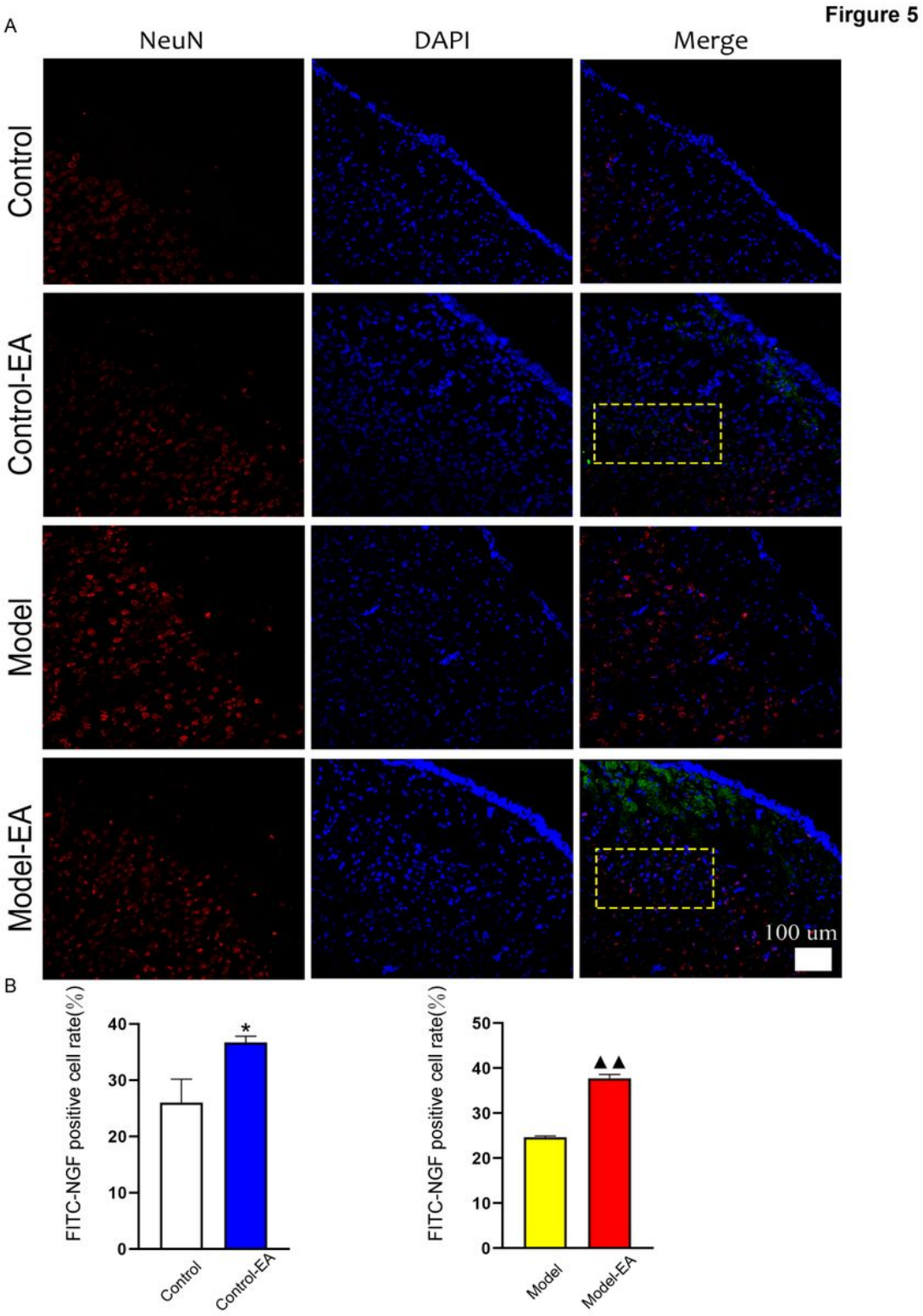

Figure 5

EA stimulation induces FITC-NGF uptake by prefrontal neurons through blood vessels. (A) Fluorescence images showing that FITC-NGF uptake by prefrontal neurons in the control-EA group, and model-EA group

in the prefrontal cortex, but control and model group had no obvious phenomenon. Positive cells were shown in the yellow dotted box. (B) FITC-NGF uptake by prefrontal neurons in control, control-EA, model and model-EA group. The mean positive cell rate was used to assess the uptake of FITC-NGF by neurons. *P<0.05, control vs control-EA; ▲▲P<0.01, model vs model-EA; n = 5/group.

Firgure 6

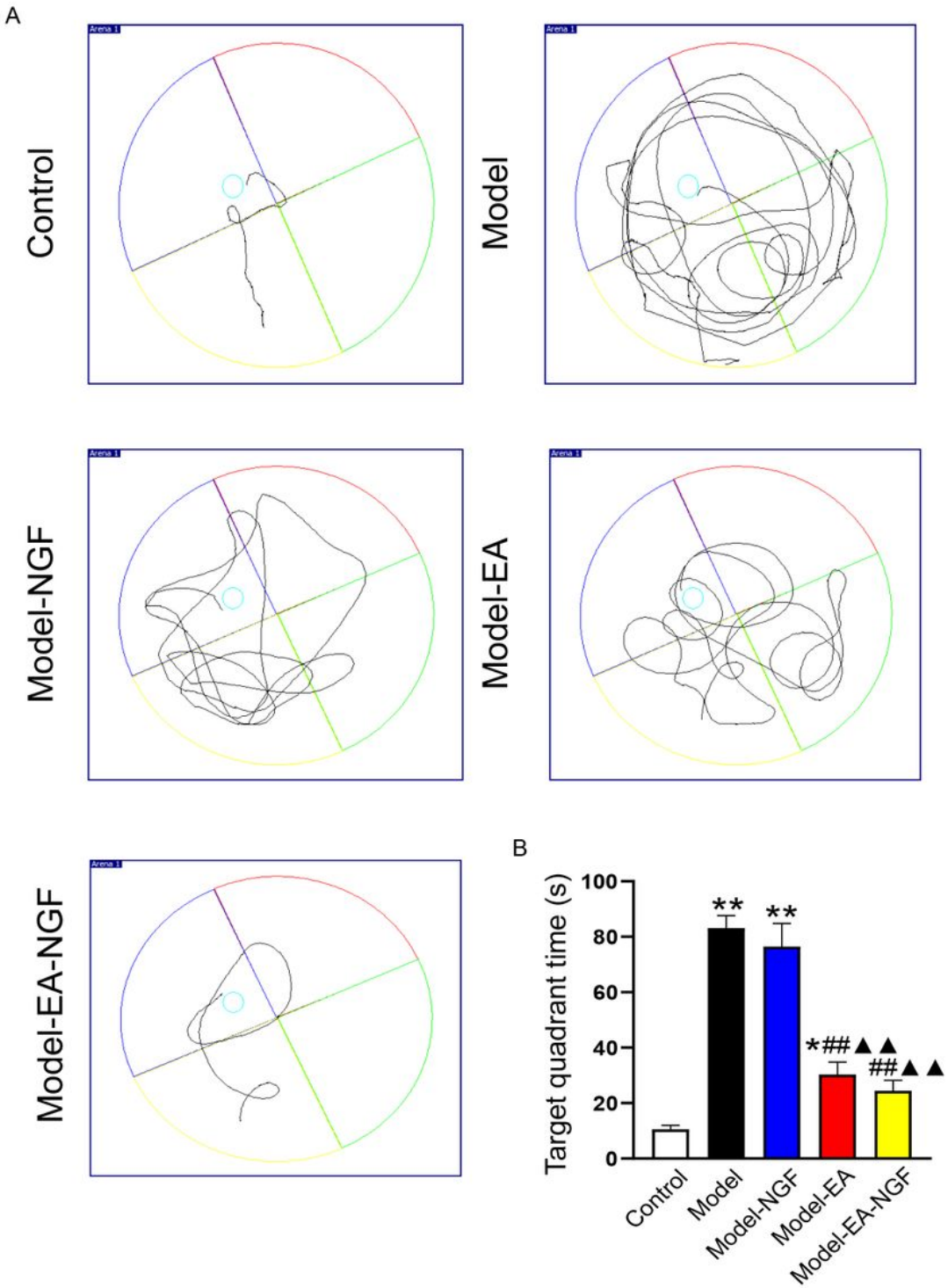

Figure 6

Induction of NGF entry into the brain by EA can promote learning ability. (A) Trajectories diagram of finding target platform in control, model, model-NGF, model-EA and model-EA-NGF group. (B) Time on latency of finding target platform in each group; *P<0.05, **P<0.01, compared with control group; ##P<0.01, compared with model group; ▲▲P<0.01, compared with model-NGF; n = 5/group.

Firgure 7

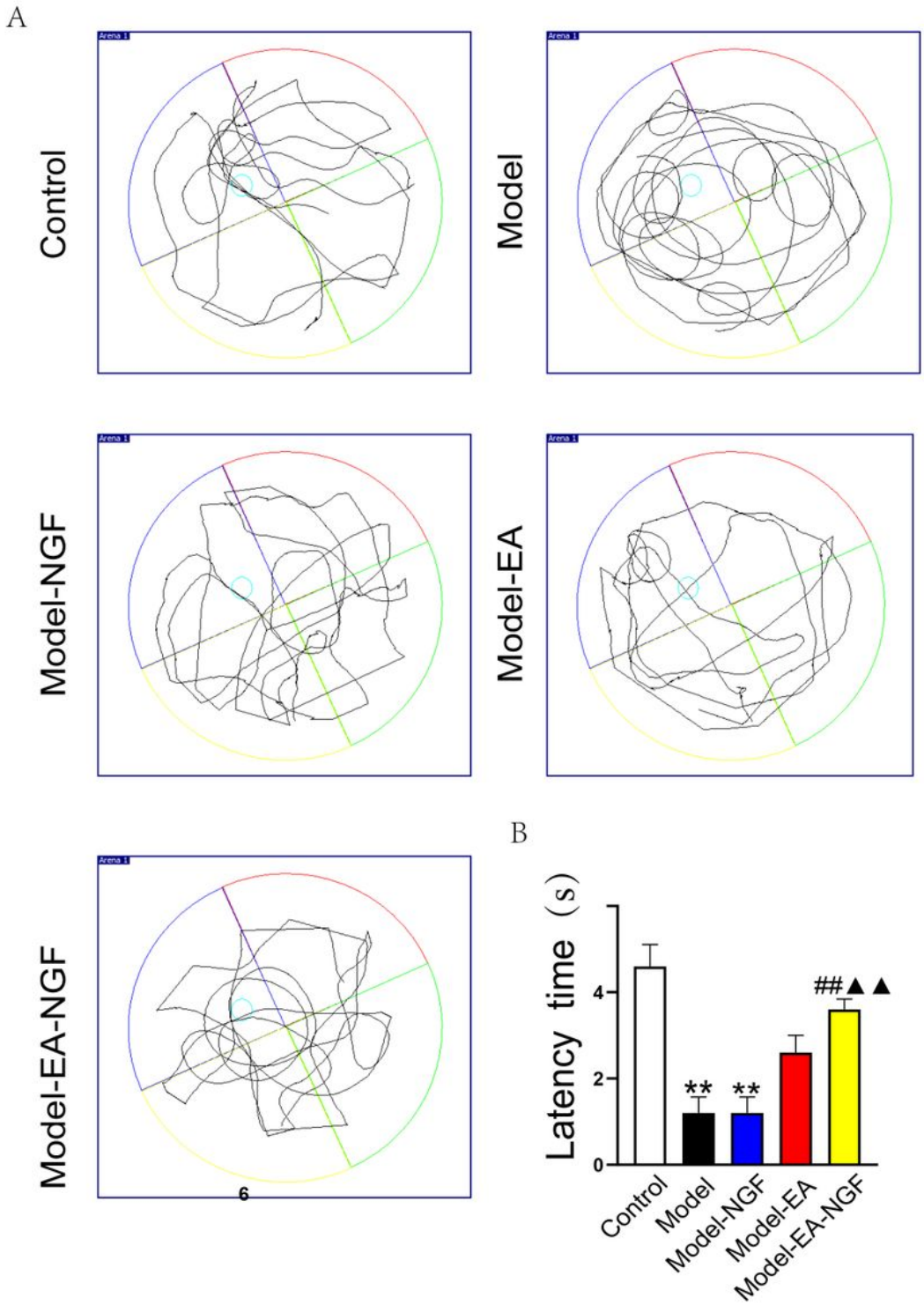

Figure 7

Induction of NGF entry into the brain by EA can promote memory ability. (A) Trajectories diagram of crossing removed platform in control, model, model-NGF, model-EA and model-EA-NGF group. (B) Times of crossing removed platform in each group in a probe trail; **P<0.01, compared with control; ##P<0.01, compared with model; ▲▲P<0.01, compared with model-NGF; n = 5/group.

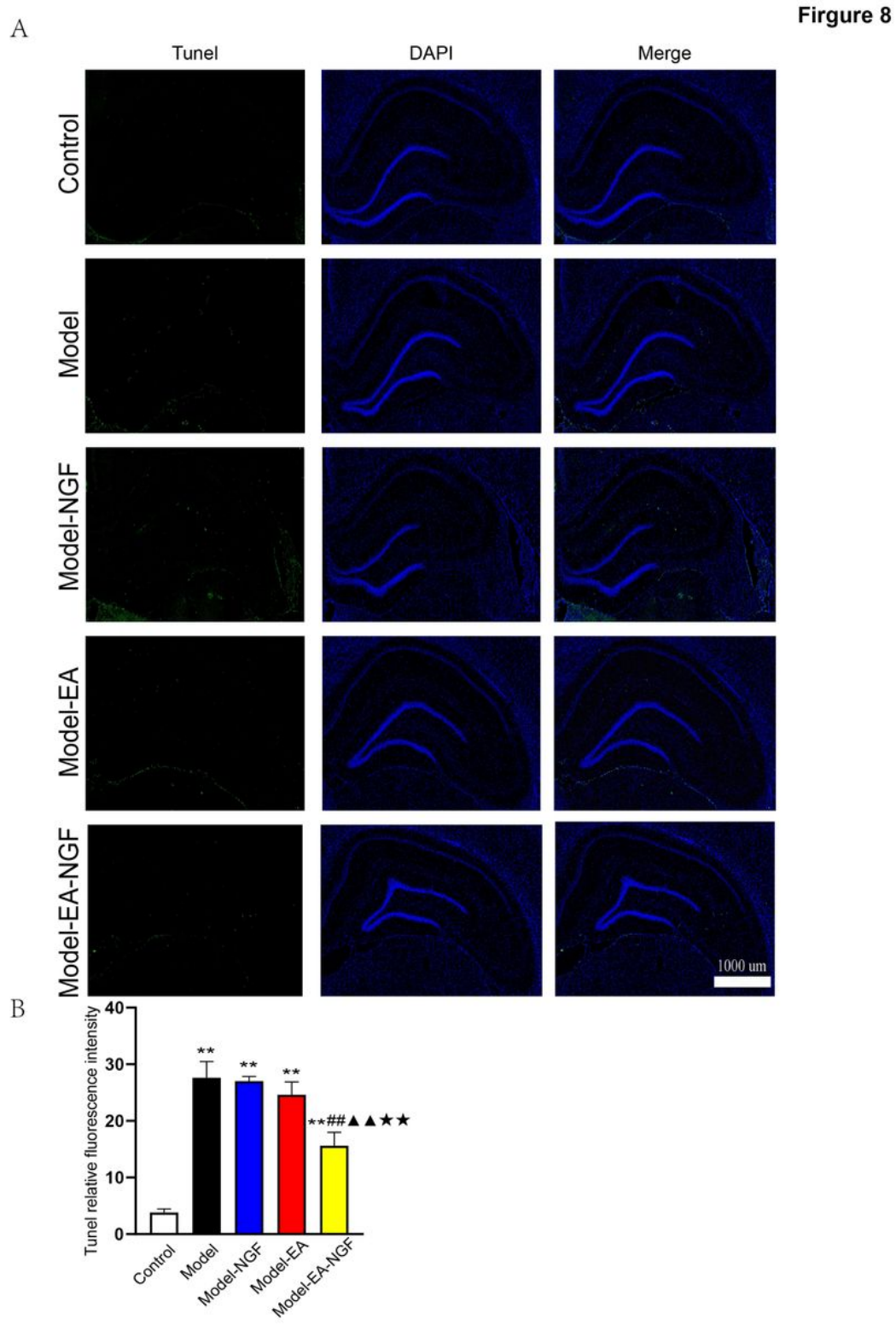

Figure 8

Apoptosis of neurons in the hippocampus. (A) Fluorescence images showing TUNEL staining in control, model, model-NGF, model-EA and model-EA-NGF group. (B) Fluorescence analysis of apoptosis levels; **P<0.01, compared with control; ##P<0.01, compared with model; ▲▲P<0.01 compared with model-NGF; ▯▯P<0.01, compared with model-EA-NGF; n = 5/group.

Supplementary Files

This is a list of supplementary files associated with this preprint. Click to download.

- SupplementaryFigure.pdf